Optical tuning of nonlinear dynamics induced by light in nematic liquid crystals

E. Brasselet[1,2]*
[1]*Laboratoire de Photonique Quantique et Moléculaire, Ecole Normale Supérieure de Cachan, 61 Avenue du Président Wilson, 94235 Cachan Cedex, France*
[2]*Département de Physique, de Génie Physique, et d'Optique, Université Laval, Cité Universitaire, Québec G1K7P4, Canada*
(Received 30 October 2003; published 27 February 2004)

We study optical control of the nonlinear dynamics generated by an ordinary polarized light at a small angle of incidence in a nematic liquid crystal film. Recent experiments have demonstrated the possibility of modifying the molecular reorientation dynamics by the addition of a weak incoherent beam orthogonally polarized to the pump beam. We present a theoretical model for the director dynamics and we demonstrate the possibility to tune the complexity of the dynamics (optical tuning) using the weak beam intensity as a control parameter. The generation of new dynamical regimes, not observed in the single beam geometry, is also predicted. Finally, interpretation of optical tuning effects is discussed on the basis of an effective model.

DOI: 10.1103/PhysRevE.69.021712 PACS number(s): 42.70.Df, 42.65.−k, 61.30.Gd

I. INTRODUCTION

The optical field induced reorientation of liquid crystal molecules is a well known phenomenon that has been thoroughly investigated for more than two decades [1–3]. Particular attention has been devoted to describing the interaction of a light beam with a nematic liquid crystal (NLC), i.e., an optically uniaxial anisotropic medium characterized by a local optical axis called a director. Of the great variety of light–matter interaction geometries, some of them have demonstrated the possibility to generate reorientation dynamics [4], and this is closely related to the exchange of spin angular momentum transfer between light and NLCs [5]. One such configuration is an elliptically polarized beam at normal incidence on a homeotropically aligned NLC, with the director perpendicular to the substrates of the sample. In that case, several different limit cycle behaviors are observed such as oscillation, nutation and precession regimes [6,7]. The particular situation where the excitation beam is circularly polarized exhibits a peculiar sequence of transitions between periodic and quasiperiodic regimes [8–10]. Another configuration, with a light beam having ordinary linear polarization at a small angle between the unperturbed director and light wave vector, is known to produce a peculiar route to chaos via a cascade of gluing bifurcations [11–13].

Optical control of the director dynamics was first demonstrated by monitoring the total angular momentum of the excitation light field using two incoherent circularly polarized beams of opposite angular momentum [14]. There, the precession regime is initially induced by a circularly polarized beam and the angular velocity is controlled by varying the intensity of the second beam. This approach was then extended to control local angular momentum deposition, thereby allowing the generation of macroscopic chiral order in achiral liquid crystals [15] and optical control of the multistability [16]. More recently, experiments for an excitation beam with ordinary linear polarization at oblique incidence (OPOI) have demonstrated the possibility of modifying the molecular reorientation dynamics by addition of a weak incoherent beam orthogonally polarized to the pump beam [17]. Since chaotic dynamics are expected in such a geometry, optical control here is a particularly interesting prospect. Qualitative comparison of experimental data with theory was restricted to a generic model with the same bifurcation scenario for a given set of parameters but without a direct link to the system, therefore limiting the physical interpretation [17].

In the present work, we develop a set of ordinary differential equations (ODEs) that describe optical control of the dynamics with a weak additional beam in OPOI geometry. This control beam is collinear, incoherent and orthogonally polarized with respect to the pump electric field. The copropagating geometry [Fig. 1(b)] was chosen for the purpose of simple demonstration. The main result of the model is a

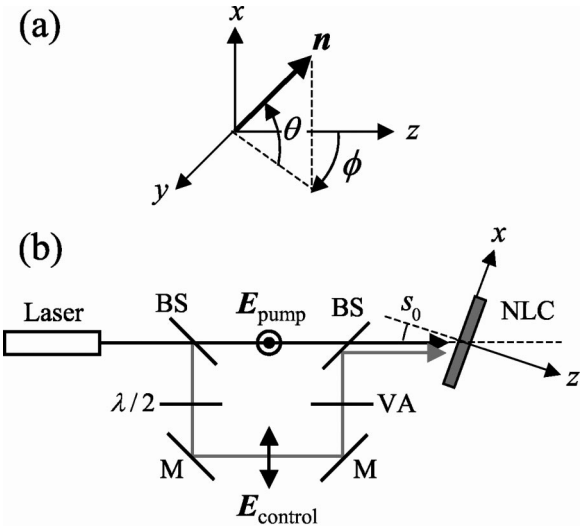

FIG. 1. (a) Definition of the director $\boldsymbol{n} = (\sin\theta, \cos\theta\sin\phi, \cos\theta\cos\phi)$ in the Cartesian coordinate system (x,y,z). (b) Interaction geometry. BS, beam splitter; M, mirror; VA, variable attenuator; λ/2, half-wave plate; NLC, nematic liquid crystal film; $\boldsymbol{E}_{\text{pump}}$, electric field of the *S*-polarized pump beam; $\boldsymbol{E}_{\text{control}}$, electric field of the *P*-polarized control beam; s_0, incidence angle of the beams.

*Email address: ebrassel@lpqm.ens-cachan.fr

description of the possibility to control the complexity of the dynamics by a procedure that amounts to an increase in intensity of the control beam. We call this effect ''optical tuning'' in the sense that initial director motion on a period-n orbit on a Poincaré surface of section can be brought to a period-m orbit with $m<n$ once control is activated. On the other hand, starting from a chaotic regime the system can be trapped in a period-n orbit or even a new regime that is not accessible with a single beam excitation. Moreover, in an attempt to understand the physical mechanism of the optical stabilization phenomenon, we propose a corresponding single beam model where an *effective* control parameter is used instead of the control beam intensity.

II. MODEL

We consider the situation depicted in Fig. 1, where an ordinary pump beam with linear polarization impinges on the NLC sample at small angle s_0. The copropagating control beam is linearly polarized in the incidence plane (x,z). For the sake of simplicity, we assume infinite plane waves and thus we consider solutions that only depend on the spatial coordinate z and time t. This assumption could prevent quantitative comparison with experimental observations if the beam size is less than the cell thickness, for which more delicate treatment is necessary [10].

The director is described by the angles θ and ϕ, $\boldsymbol{n}=(\sin\theta,\cos\theta\sin\phi,\cos\theta\cos\phi)$ [Fig. 1(a)], and the strong anchoring conditions $[\theta(0,t)=\theta(L,t)=\phi(0,t)=\phi(L,t)=0]$ allow one to expand these angles into Fourier series,

$$\theta(z,t)=\sum_{n=1}^{\infty}\theta_n(t)\sin(n\pi z/L), \tag{1}$$

$$\phi(z,t)=\sum_{n=1}^{\infty}\phi_n(t)\sin(n\pi z/L). \tag{2}$$

The system of equations that describes the director dynamics is obtained from the fundamental equations of liquid crystals and those of electromagnetic waves by writing the balance of viscous, elastic and electromagnetic torque exerted on the director [18]. By projecting these equations on modes θ_n and ϕ_n, a set of ODEs is obtained. For the simplest nonlinear model and assuming small reorientation amplitude $(\theta,\phi\ll 1)$ we expand all functions as a power series in these angles up to third order. Finally, by retaining a finite number of modes for each angles we have a set of coupled, first order, nonlinear ODEs for variables $\phi_1,\ldots,\phi_N$ and $\theta_1,\ldots,\theta_M$. One can show that the minimum number of modes required to properly describe the case of a single *o*-polarized excitation beam corresponds to $N=2$ and $M=1$ since ϕ_1 is the only linearly unstable mode for excitation intensities not too high above the primary instability and that three variables suffice to obtain chaotic behavior [19]. However, in the present case, θ_1 is always unstable due to the second *e*-polarized beam ($c_{0000}\neq 0$; see the Appendix) therefore the second mode in the θ direction, θ_2, must also be retained $(N=2,\ M=2)$. Finally, the resulting dynamical system is described by the following set of four coupled ODEs:

$$\tau\frac{\partial}{\partial t}\begin{pmatrix}\phi_1\\ \phi_2\\ \theta_1\\ \theta_2\end{pmatrix}=\sum_{\alpha,\beta,\gamma,\delta}\begin{pmatrix}a_{\alpha\beta\gamma\delta}\\ b_{\alpha\beta\gamma\delta}\\ c_{\alpha\beta\gamma\delta}\\ d_{\alpha\beta\gamma\delta}\end{pmatrix}\phi_1^{\alpha}\phi_2^{\beta}\theta_1^{\gamma}\theta_2^{\delta}, \tag{3}$$

with

$$0\leqslant\alpha+\beta+\gamma+\delta\leqslant 3 \tag{4}$$

(α, β, γ, and δ are integers), where $\tau=(\gamma L^2)/(\pi^2K_3)$ is a characteristic reorientation time with L the cell thickness, γ the orientational viscosity and K_3 the bend elastic constant. Coefficients a, b, c and d are calculated using the formalism presented in Ref. [19] and are expressed in terms of the normalized intensity parameters ρ_1 and ρ_2,

$$\rho_1=\frac{I_1}{I_F},\quad \rho_2=\frac{I_2}{I_F}, \tag{5}$$

where $I_1=|\boldsymbol{E}_{\text{pump}}|^2$ is the intensity of the pump beam, $I_2=|\boldsymbol{E}_{\text{control}}|^2$ is the intensity of the control beam. The intensity $I_F=(8\pi\epsilon_{\parallel}\pi^2K_3)/(\epsilon_a\epsilon_{\perp}L^2)$ is the Fréedericksz transition threshold for linearly polarized excitation at normal incidence where $\epsilon_{\perp}$ ($\epsilon_{\parallel}$) is the dielectric permittivity perpendicular (parallel) to $\boldsymbol{n}$ at optical frequency and $\epsilon_a=\epsilon_{\parallel}-\epsilon_{\perp}$. We further define the parameters $\eta=\epsilon_a/\epsilon_{\perp}$, $s=s_0/\epsilon_{\perp}^{1/2}$ and $\kappa=(L/\lambda)[s^2\epsilon_{\perp}^{1/2}\eta/(1+\eta)]$ where λ is the wavelength of the light field. The physical meaning of κ comes from the observation that the phase shift between an *o* and an *e* wave at the output of the cell $(z=L)$, when there is no reorientation $(\theta=\phi=0)$, is well approximated by $\kappa\pi$ [19]. Finally, we have used the ratios $K_1/K_3=2/3$ and $K_2/K_3=1/2$ of the Frank elastic constants that are valid for NLC $E7$ at room temperature. The expressions for coefficients a, b, c and d are given in the Appendix within the limit of $s^2\ll 1$ and $\kappa^2\ll 1$. Our simulations are performed with parameters $s_0=7°$, $\eta=0.338$, $\lambda=514.5$ nm and $L=50$ μm for which $s^2=6.6\times10^{-3}$ and $\kappa^2=6.0\times10^{-2}$. As expected, one can verify that system (3) reduces to the one in Ref. [19] by setting $\rho_2=0$ and $\theta_2=0$.

III. SIMULATIONS

First, we studied, the bifurcation scenario without the control beam $(\rho_2=0)$ and, as was predicted in Refs. [12] and [19] we found that the presence of mode θ_2 does not alter significantly the dynamics with respect to the minimal model (when $\rho_2=0$) where only ϕ_1, ϕ_2 and θ_1 are retained [12,19]. More precisely, we found that a transition to chaos via a cascade of gluing bifurcations occurs although the intermediate transition thresholds are slightly lowered with respect to the three mode model when θ_2 is taken into account (Table I). In Table I, we report the successive transition thresholds starting from $\rho_1=0$ and increasing the excitation

TABLE I. Calculated values of the successive transitions thresholds for the three mode model (ϕ_1,ϕ_2,θ_1) and four mode model $(\phi_1,\phi_2,\theta_1,\theta_2)$.

Transition threshold	Three mode model	Four mode model
$\rho^{(c)}$	1.063	1.063
$\rho^{(0)}$	1.717	1.682
$\rho^{(1)}$	1.809	1.773
$\rho^{(2)}$	1.947	1.902

intensity. The threshold value $\rho^{(c)}$ corresponds to destabilization of the initial homeotropic state to a stationary reoriented state and $\rho^{(0)}$ refers to the supercritical Hopf bifurcation which leads to the appearance of two limit cycles that are mutual images under symmetry of $\phi_n \rightarrow -\phi_n$ $(\mathcal{S})$ [12,19]. The values $\rho^{(n\geqslant 1)}$ are the gluing bifurcations thresholds where two asymmetric limit cycles that are mutual images under $\mathcal{S}$ merge into a single double-length limit cycle at the origin [12,19]. The limit cycles above $\rho_1=\rho^{(n)}$ $(n\leqslant 2)$ are summarized in Fig. 2 where projections of the director trajectory in the planes (ϕ_1,θ_1) (left column) and (ϕ_2,θ_2) (right column) are displayed.

When the control beam is activated $(\rho_2\neq 0)$, the initial director dynamics may be significantly altered even for small values of the ratio between the control and the pump beam intensities,

$$R=\frac{I_2}{I_1}. \tag{6}$$

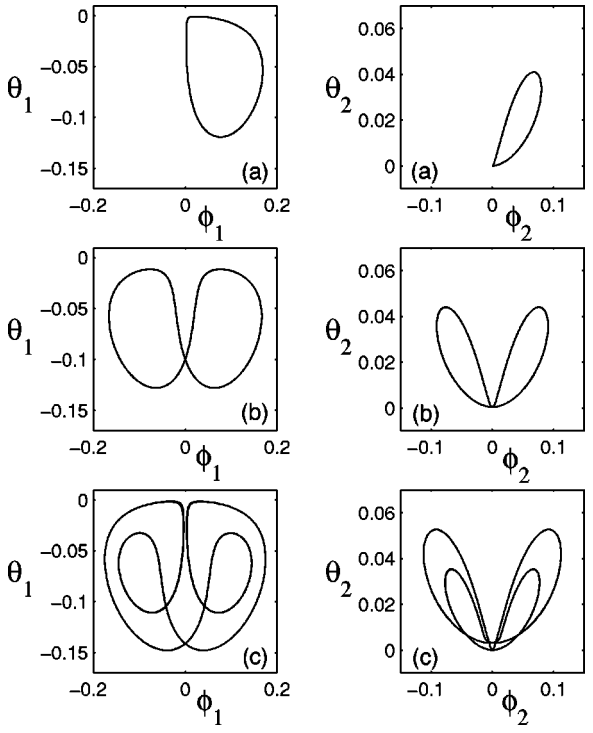

FIG. 2. Projections of the director trajectory in planes ϕ_1,θ_1 (left column) and ϕ_2,θ_2 (right column) for different values of excitation intensity ρ without the control beam $(\rho_2=0)$. $\rho_1=$ (a) 1.77; (b) 1.85; (c) 1.91.

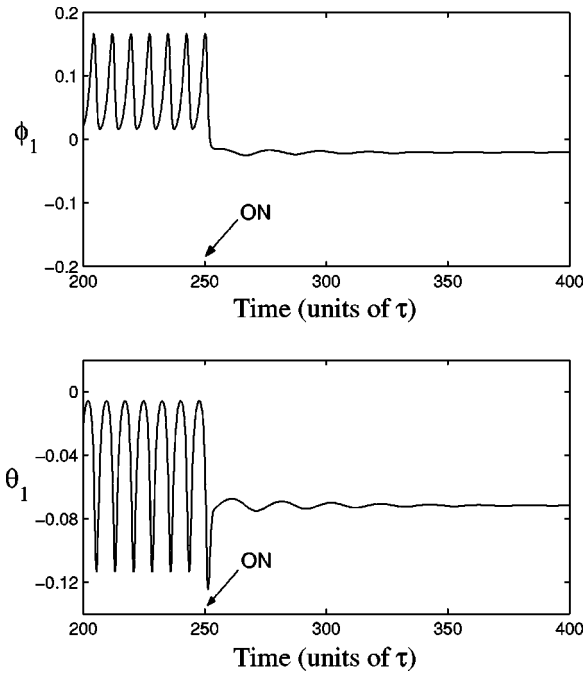

FIG. 3. Stabilization of the periodic regime below the first gluing bifurcation at $\rho_1=1.75$ in a distorted regime. The control beam intensity is activated at $t=250\tau$ with $R=0.17$ ($t_0=250\tau$ and $t_1-t_0=4\tau$; see the text). The time behavior of angles ϕ_1 (upper panel) and θ_1 (lower panel) is indicated.

This is demonstrated in Figs. 3 and 4 which represent $\theta_1(t)$ and $\phi_1(t)$ before and after the control beam has been switched on for different values of ρ_1, which is kept fixed. In Fig. 3, the limit cycle obtained at $\rho_1=1.75$ is stabilized to a fixed point that corresponds to a stationary distorted state, as observed experimentally in Ref. [17]. However, experimental stabilization was observed for values of R as small as 10^{-2} for which we did not observe stabilization in the present simulations. This discrepancy may be due to the fact that, in our case, light propagation is solved up to third order in the angles and that in Ref. [17] contrapropagating geometry was used. In fact, truncation to third angle in the angles has brought us to use a smooth $[\propto \sin^2\pi/2(t-t_0/t_1-t_0)$ where (t_0,t_1) correspond to the finite duration of the activation of the control beam] rather than a steplike profile for simulation of the addition of the second beam, but only for the case presented in Fig. 3 where the value of R is relatively large. On the other hand, a periodic regime could be driven into another periodic regime using the control beam. This is shown in Fig. 4 where a single double-length limit cycle at $\rho_1=1.80$ [Fig. 4(c)], above the first gluing bifurcation, is stabilized into a single limit cycle [Fig. 4(d)] very similar to the one obtained without control before the first gluing bifurcation [see Fig. 2(a)]. In fact, the final state can be either one of the two single limit cycles (mutual images under $\mathcal{S}$) depending on when the control beam is activated.

The chaotic regime can also be stabilized into various regimes, periodic or not. Figure 5 shows three different optically stabilized limit cycle behaviors starting from the $\rho_1=1.98$ and $\rho_2=0$. Figure 5(a) corresponds to the initial at-

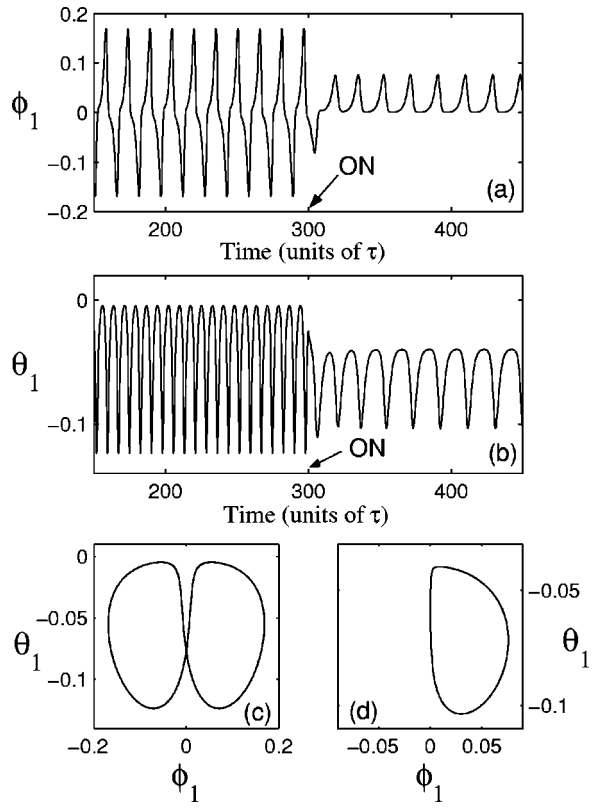

FIG. 4. Stabilization of the periodic regime between the first and the second gluing bifurcation at $\rho_1=1.80$ in another periodic regime. The control beam intensity is activated at $t=300\tau$ with $R=0.14$. (a) $\phi_1(t)$; (b) $\theta_1(t)$; (c),(d) projection of the limit cycle in plane ϕ_1,θ_1 before and after the control beam is switched on.

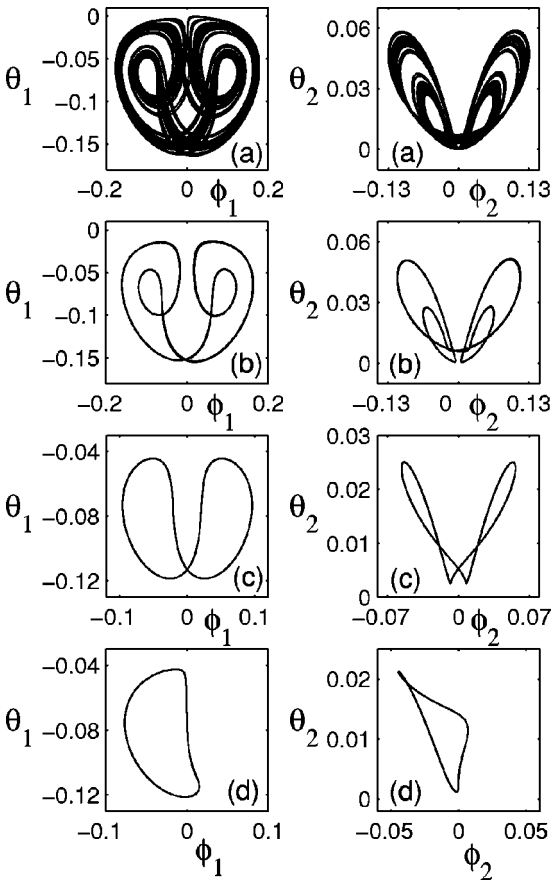

FIG. 5. Projections of the director trajectory in planes ϕ_1,θ_1 (left column) and ϕ_2,θ_2 (right column) for $\rho_1=1.98$ and different values of control beam intensity. $R=$ (a) 0; (b) 0.02; (c) 0.10; (d) 0.13.

tractor ($R=0$) while Figs. 5(b)–5(d) correspond to $R=0.02$, 0.10 and 0.13, respectively; these results are in good agreement with the observations reported in Ref. [17]. One again notes that the stabilized periodic regime is similar to the one obtained after the second gluing bifurcation in the case of $R=0.02$ [cf. Figs. 5(b) and 2(c)] to the one obtained after the first gluing bifurcation, $R=0.10$ [cf. Figs. 5(c) and 2(b)] and to the one obtained after Hopf bifurcation at $\rho=\rho^{(0)}$, $R=0.13$ [cf. Figs. 5(d) and 2(a)]. This demonstrates the possibility of tuning the initial complexity of the dynamics with a weak additional beam using R as a control parameter, and we refer to this effect as *optical tuning*. It is worth mentioning that, contrary to standard techniques that allow control of chaos using judicious small *dynamical* variations of a control parameter [20,21], the proposed method consists of the application of *static* perturbation, which brings additional nonlinearities.

Phenomenologically, the control beam reduces the degrees of freedom of the system. This can be understood qualitatively since the additional beam is *e* polarized with respect to the initial homeotropic state. In fact, the corresponding interaction geometry is thresholdless ($c_{0000}\neq 0$; see the Appendix) in contrast to the situation that corresponds to the pump beam alone. It is therefore expected that the director dynamics are constrained since $\boldsymbol{n}$ tends to be attracted towards the polarization plane of the additional beam (x,z). This is illustrated in Fig. 3, where the director is closer to the (x,z) plane (i.e., $\phi=0$ and $\theta\neq 0$) in the presence of the second beam.

Moreover, the control beam can drive the system towards regimes that cannot be observed without the second beam. For example, Fig. 6 shows a situation where the initial chaotic regime is set into a period-doubled asymmetric limit cycle using $R=0.06$. Figure 7 presents corresponding projections of the director trajectory in the planes [(ϕ_1,θ_1) and (ϕ_2,θ_2)] for the stabilized regime. The generation of a new dynamical regime also agrees with previous experimental results [17].

In an attempt to physically interpret the origin of the nonlinear behavior of the system in the presence of a weak additional *e*-polarized beam, we would like to emphasize the crucial role played by the incidence angle in director dynamics even in single *o*-polarized geometry. It was established that different bifurcation scenarios are expected, depending on the value of s_0, and that different dynamical regimes with respect to those observed in the case $s_0=7°$ eventually occur [19]. In Sec. IV, it is shown that a single beam model can be derived by using an *effective* incidence angle as a control parameter instead of the control beam intensity.

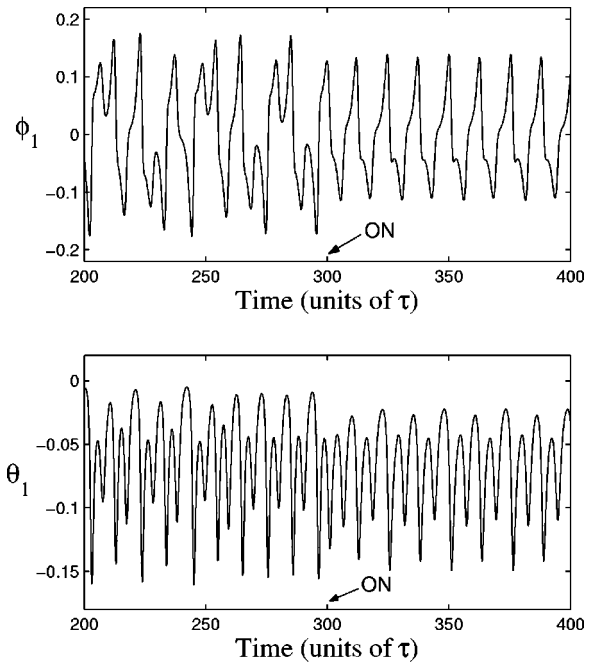

FIG. 6. Stabilization of the chaotic regime at $\rho_1=1.98$ in a period-doubled asymmetric limit cycle. The control beam intensity is activated at $t=300\tau$ with $R=0.06$. The time behavior of angles ϕ_1 (upper panel) and θ_1 (lower panel) is indicated.

IV. EFFECTIVE MODEL

The main idea behind the effective single beam model is to consider separately the action of the pump and the control beam on the NLC although both act simultaneously in a real system. First, we focus on the effect of a weak (with respect to I_F) *e*-polarized beam with angle of incidence s_0. It is known that the corresponding reorientation process is thresholdless and that, in its final state, the director's profile is stationary and lies in the plane of incidence [$\phi=0$, $\theta=\theta(z)$], as presented in Fig. 8(a) [1]. Then, the (collinear) pump beam is considered to interact with the latter reorientation profile $\theta(z)$. In that case, the local angle of incidence between the z axis and wave vector $\boldsymbol{k}$ is therefore expressed as [Fig. 8(b)]

$$s_{\mathrm{local}}(z)=s-\theta(z). \tag{7}$$

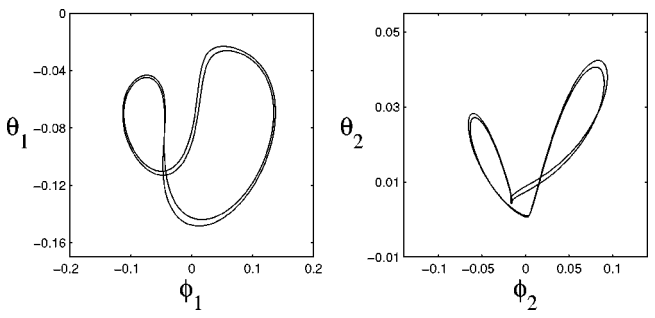

FIG. 7. Projection of the director trajectory in planes ϕ_1,θ_1 (left) and ϕ_2,θ_2 (right) in the regime obtained from stabilization of the dynamics at $\rho_1=1.98$ with $R=0.06$ (see Fig. 6).

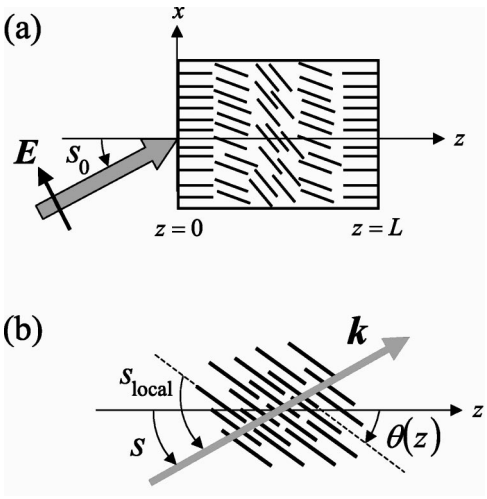

FIG. 8. (a) Reorientation of the NLC by an *e* beam with angle of incidence s_0. (b) Local angle $s_{\mathrm{local}}(z)=s-\theta(z)$.

From a qualitative point of view, simultaneous action of the collinear *o*- and *e*-polarized beams can thus be considered to be that of a single *o* beam with an effective incident angle that depends on the reorientation amplitude induced by the *e*-beam alone. To this end, we introduce the effective angle of incidence,

$$s_{\mathrm{eff}}\equiv\langle s_{\mathrm{local}}\rangle_z, \tag{8}$$

where the angled brackets refer to spatial averaging along the z direction. Then, a single beam analog ($\rho_2=0$) of the original problem with parameters ρ_1, ρ_2 and s is obtained using

$$[\rho_1,\rho_2,s]\Leftrightarrow[\rho_1,0,s_{\mathrm{eff}}(\rho_2,s)], \tag{9}$$

where the effective angle $s_{\mathrm{eff}}(\rho_2,s)$ corresponds to the situation where the NLC is reoriented by the *e* beam alone at angle of incidence $s_0=s\epsilon_\perp^{1/2}$ with intensity ρ_2. From the above discussion, we have

$$s_{\mathrm{eff}}(\rho_2,s)=s-\frac{1}{L}\int_0^L\theta(z)_{\rho_1=0}\,dz, \tag{10}$$

where $\theta(z)_{\rho_1=0}$ is the reorientation profile that corresponds to $\rho_1=0$, ρ_2 and s_0. The latter in-plane ($\phi=0$) reorientation profile is the solution of the following homogeneous nonlinear system of two equations [see Eqs. (3) and (4)]:

$$\sum_{\gamma,\delta}\begin{pmatrix}c_{00\gamma\delta}\\ d_{00\gamma\delta}\end{pmatrix}{\theta_1}^\gamma{\theta_2}^\delta=0, \tag{11}$$

with

$$0\leqslant\gamma+\delta\leqslant3. \tag{12}$$

Figure 9(a) shows the solution of Eqs. (11) and (12) in the range of $0\leqslant\rho_2\leqslant0.35$ and the effective angle of incidence,

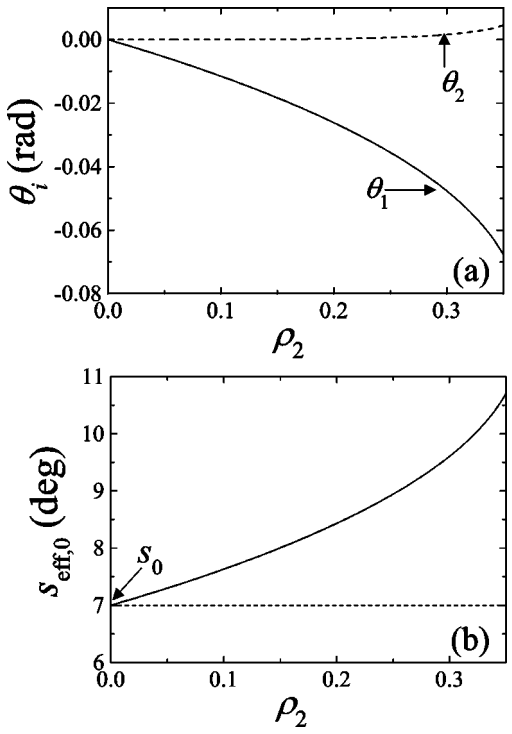

FIG. 9. (a) Calculated θ_1 (solid line) and θ_2 (dashed line) vs ρ_2 for $\rho_1=0$ and $s_0=7°$. (b) Calculated effective angle of incidence $s_{\mathrm{eff},0}$ vs ρ_2 under the same conditions as those in (a).

$s_{\mathrm{eff},0}$, is calculated as a function of ρ_2 using Eq. (10) when $s_0=7°$ [Fig. 9(b)]. Typically, the effective angle can increase by more than 1° with respect to the real angle of incidence even with moderate values of ρ_2 [Fig. 9(b)]. This allows us to understand qualitatively the results in Sec. III since the dynamics are very sensitive to the angle of incidence [19] and that, from the equivalence given by Eq. (9), it is possible to describe optical stabilization using the single beam model ($\rho_2=0$) but varying the angle of incidence. For instance, Fig. 10 shows the analog of the stabilization of the chaotic regime at $\rho_1=1.98$ and $s_0=7°$ with $R=0.1$ [see Fig. 5(c)] using the effective model. In that case, it corresponds to an increase in incidence angle by the amount $s_{\mathrm{eff},0}(0.198,s_0)-s_0=1.4°$, but keeping $\rho_1=1.98$ and $\rho_2=0$. The final state obtained in the effective model is very similar to the one obtain in the original model where the angle of incidence is fixed and the value of ρ_2 is changed from 0 to 0.198 [cf. Figs. 10(d) and 5(c)]; this confirms our interpretation of the stabilization phenomenon.

V. CONCLUSION

In this work, we have studied optical control of the director dynamics generated by an ordinary polarized light at a small angle of incidence in a homeotropic nematic liquid crystal film by adding a collinear orthogonally polarized beam with respect to the pump beam. A set of ordinary differential equations was obtained and the possibility to tune the complexity of the dynamics using the control beam intensity as a control parameter was demonstrated. New dynamical regimes not observed in single beam geometry were also predicted. The results obtained agree with previous experimental observations and physical interpretation of the stabilization phenomenon was proposed through an effective model, in which the angle of incidence is viewed as the control parameter and only one beam is used. We hope this work will be useful for systematic analysis of previous and future experimental results.

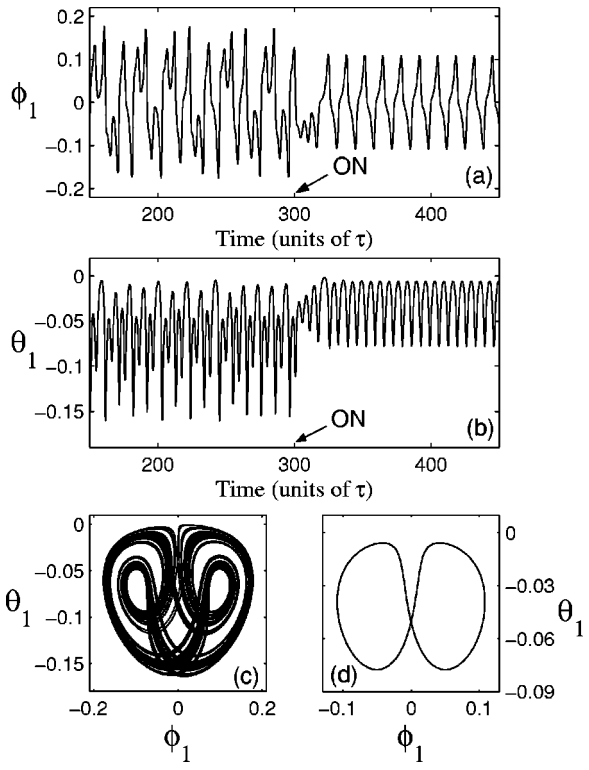

FIG. 10. Stabilization of the chaotic regime in the effective model that corresponds to $\rho_1=1.98$, $R=0.1$ and $s_0=7°$ in the original model [see Fig. 5(c)]. The incidence angle is set to the new value, $s_{\mathrm{eff},0}(0.198,s_0)=8.4°$, at $t=300\tau$ when effective control is activated. (a) $\phi_1(t)$; (b) $\theta_1(t)$; (c),(d) projection of the director trajectory in plane ϕ_1,θ_1 before and after the angle is changed.

ACKNOWLEDGMENTS

The author is grateful to G. Cipparrone for communication of a preprint version of Ref. [17] prior to publication and thanks L. J. Dubé and T. V. Galstian for helpful discussions and comments on the manuscript.

APPENDIX

Here we give explicit expressions for the nonzero coefficients $a_{\alpha\beta\gamma\delta}$, $b_{\alpha\beta\gamma\delta}$, $c_{\alpha\beta\gamma\delta}$ and $d_{\alpha\beta\gamma\delta}$ introduced in Eq. (3) for $\alpha+\beta+\gamma+\delta\leqslant 3$ with α, β, γ and δ integers:

$$a_{1000}=-1+\rho_1[1-\kappa^2]-\rho_2\left[\frac{s^2}{1+\eta}-\kappa^2\right], \tag{A1}$$

$$a_{0100}=-(\rho_1-\rho_2)\kappa^2, \tag{A2}$$

$$a_{1010}=\rho_1\pi\frac{\kappa^2}{s}+\rho_2\left[\frac{16}{3\pi}\frac{s}{1+\eta}-\pi\frac{\kappa^2}{s}\right], \tag{A3}$$

$$a_{0110}=(\rho_1-\rho_2)\frac{9\pi^2+256}{36\pi}\frac{\kappa^2}{s}, \tag{A4}$$

$$a_{0101}=\rho_1\frac{45\pi^2-128}{90\pi}\frac{\kappa^2}{s}+\rho_2\left[\frac{64}{15\pi}\frac{s}{1+\eta}-\frac{45\pi^2-128}{90\pi}\frac{\kappa^2}{s}\right], \tag{A5}$$

$$a_{1200}=\frac{5}{6}+\rho_1\left[\frac{2\eta-1}{1+\eta}+\frac{7}{8}\frac{\kappa^2}{s^2}\right]-\rho_2\frac{7}{8}\frac{\kappa^2}{s^2}, \tag{A6}$$

$$a_{3000}=\frac{1}{6}+\rho_1\left[\frac{2\eta-1}{2(1+\eta)}-\frac{\kappa^2}{2s^2}\right]+\rho_2\frac{\kappa^2}{2s^2}, \tag{A7}$$

$$a_{1020}=-\frac{1}{3}+\rho_1\left[\frac{3\eta}{4(1+\eta)}-\frac{141+4\pi^2}{48}\frac{\kappa^2}{s^2}\right]+\rho_2\left[\frac{3\eta(2+\eta)}{4(1+\eta)}+\frac{141+4\pi^2}{48}\frac{\kappa^2}{s^2}\right], \tag{A8}$$

$$a_{0300}=(\rho_1-\rho_2)\frac{\kappa^2}{2s^2}, \tag{A9}$$

$$a_{1002}=\frac{5}{4}+\rho_1\left[\frac{\eta}{2(1+\eta)}-\frac{8}{9}\frac{\kappa^2}{s^2}\right]+\rho_2\left[\frac{\eta(2+\eta)}{2(1+\eta)}+\frac{8}{9}\frac{\kappa^2}{s^2}\right], \tag{A10}$$

$$a_{2100}=(\rho_1-\rho_2)\frac{\kappa^2}{4s^2}, \tag{A11}$$

$$a_{0120}=-(\rho_1-\rho_2)\frac{127}{36}\frac{\kappa^2}{s^2}, \tag{A12}$$

$$a_{0102}=-(\rho_1-\rho_2)\frac{7}{18}\frac{\kappa^2}{s^2}, \tag{A13}$$

$$a_{0111}=-\frac{53}{12}+\rho_1\left[\frac{\eta}{1+\eta}-\frac{487+24\pi^2}{288}\frac{\kappa^2}{s^2}\right]+\rho_2\left[\frac{\eta(2+\eta)}{1+\eta}+\frac{487+24\pi^2}{288}\frac{\kappa^2}{s^2}\right], \tag{A14}$$

$$b_{0100}=-4+\rho_1\left[1+\frac{3}{4}\kappa^2\right]-\rho_2\left[\frac{s^2}{1+\eta}+\frac{3}{4}\kappa^2\right], \tag{A15}$$

$$b_{1000}=(\rho_1-\rho_2)\kappa^2, \tag{A16}$$

$$b_{0110}=-\rho_1\frac{64}{9\pi}\frac{\kappa^2}{s}+\rho_2\left[\frac{64}{15\pi}\frac{s}{1+\eta}+\frac{64}{9\pi}\frac{\kappa^2}{s}\right], \tag{A17}$$

$$b_{1010}=-(\rho_1-\rho_2)\frac{9\pi^2+256}{36\pi}\frac{\kappa^2}{s}, \tag{A18}$$

$$b_{1001}=\rho_1\frac{45\pi^2-128}{90\pi}\frac{\kappa^2}{s}+\rho_2\left[\frac{64}{15\pi}\frac{s}{1+\eta}-\frac{45\pi^2-128}{90\pi}\frac{\kappa^2}{s}\right], \tag{A19}$$

$$b_{1011}=-\frac{17}{12}+\rho_1\left[\frac{\eta}{1+\eta}-\frac{487+24\pi^2}{288}\frac{\kappa^2}{s^2}\right]+\rho_2\left[\frac{\eta(2+\eta)}{1+\eta}+\frac{487+24\pi^2}{288}\frac{\kappa^2}{s^2}\right], \tag{A20}$$

$$b_{3000}=(\rho_1-\rho_2)\frac{\kappa^2}{4s^2}, \tag{A21}$$

$$b_{1200}=-(\rho_1-\rho_2)\frac{3}{2}\frac{\kappa^2}{s^2}, \tag{A22}$$

$$b_{1020}=(\rho_1-\rho_2)\frac{127}{36}\frac{\kappa^2}{s^2}, \tag{A23}$$

$$b_{1002}=(\rho_1-\rho_2)\frac{7}{18}\frac{\kappa^2}{s^2}, \tag{A24}$$

$$b_{2100}=\frac{5}{6}+\rho_1\left[\frac{2\eta-1}{1+\eta}-\frac{9}{8}\frac{\kappa^2}{s^2}\right]+\rho_2\frac{9}{8}\frac{\kappa^2}{s^2}, \tag{A25}$$

$$b_{0300}=\frac{2}{3}+\rho_1\left[\frac{2\eta-1}{2(1+\eta)}-\frac{5}{8}\frac{\kappa^2}{s^2}\right]+\rho_2\frac{5}{8}\frac{\kappa^2}{s^2}, \tag{A26}$$

$$b_{0120}=\frac{5}{4}+\rho_1\left[\frac{\eta}{2(1+\eta)}+\frac{185}{72}\frac{\kappa^2}{s^2}\right]+\rho_2\left[\frac{\eta(2+\eta)}{2(1+\eta)}-\frac{185}{72}\frac{\kappa^2}{s^2}\right], \tag{A27}$$

$$b_{0102}=-\frac{4}{3}+\rho_1\left[\frac{3\eta}{4(1+\eta)}-\frac{45+16\pi^2}{192}\frac{\kappa^2}{s^2}\right]+\rho_2\left[\frac{3\eta(2+\eta)}{4(1+\eta)}+\frac{45+16\pi^2}{192}\frac{\kappa^2}{s^2}\right], \tag{A28}$$

$$c_{0000}=-\rho_2\frac{4s}{\pi}, \tag{A29}$$

$$c_{0010}=-1+\rho_2, \tag{A30}$$

$$c_{0020}=\rho_2\frac{16}{3\pi}\left[\frac{s}{1+\eta}-4\frac{\kappa^2}{s}\right], \tag{A31}$$

$$c_{0011}=-\rho_2\frac{64}{3\pi}\frac{\kappa^2}{s}, \tag{A32}$$

$$c_{0002}=\rho_2\frac{64}{15\pi}\left[\frac{s}{1+\eta}-2\frac{\kappa^2}{s}\right], \tag{A33}$$

$$c_{2000}=-\rho_1\frac{16-\pi^2}{2\pi}\frac{\kappa^2}{s}+\rho_2\left[\frac{4}{3\pi}\frac{1-\eta}{1+\eta}s-\frac{3\pi^2-16}{6\pi}\frac{\kappa^2}{s}\right], \tag{A34}$$

$$c_{0200}=-\rho_1\frac{32}{9\pi}\frac{\kappa^2}{s}+\rho_2\left[\frac{16}{15\pi}\frac{1-\eta}{1+\eta}s+\frac{64}{45\pi}\frac{\kappa^2}{s}\right], \tag{A35}$$

$$c_{1100}=-\rho_1\frac{256-9\pi^2}{36\pi}\frac{\kappa^2}{s}-\rho_2\frac{9\pi^2-64}{36\pi}\frac{\kappa^2}{s}, \tag{A36}$$

$$c_{2010}=\frac{5}{12}-\rho_1\left[\frac{3}{4(1+\eta)}-\frac{147-4\pi^2}{48}\frac{\kappa^2}{s^2}\right]+\rho_2\left[\frac{3\eta}{4(1+\eta)}+\frac{45+4\pi^2}{48}\frac{\kappa^2}{s^2}\right], \tag{A37}$$

$$c_{0210}=\frac{13}{4}-\rho_1\left[\frac{1}{2(1+\eta)}-\frac{185}{72}\frac{\kappa^2}{s^2}\right]+\rho_2\left[\frac{\eta}{2(1+\eta)}-\frac{10}{9}\frac{\kappa^2}{s^2}\right], \tag{A38}$$

$$c_{0030}=\frac{1}{6}+\rho_2\left[\frac{2\eta-1}{2(1+\eta)}+\frac{21}{2}\frac{\kappa^2}{s^2}\right], \tag{A39}$$

$$c_{0012}=\frac{5}{6}+\rho_2\left[\frac{2\eta-1}{1+\eta}+\frac{53}{6}\frac{\kappa^2}{s^2}\right], \tag{A40}$$

$$c_{0021}=\rho_2\frac{26}{3}\frac{\kappa^2}{s^2}, \tag{A41}$$

$$c_{0003}=\rho_2\frac{8}{3}\frac{\kappa^2}{s^2}, \tag{A42}$$

$$c_{1110}=\left(\frac{7}{2}\rho_1+\frac{1}{3}\rho_2\right)\frac{\kappa^2}{s^2}, \tag{A43}$$

$$c_{2001}=-(\rho_1-\rho_2)\frac{11}{18}\frac{\kappa^2}{s^2}, \tag{A44}$$

$$c_{0201}=(4\rho_1-\rho_2)\frac{4}{9}\frac{\kappa^2}{s^2}, \tag{A45}$$

$$c_{1101}=-\frac{5}{12}-\rho_1\left[\frac{1}{1+\eta}-\frac{665-24\pi^2}{288}\frac{\kappa^2}{s^2}\right]+\rho_2\left[\frac{\eta}{1+\eta}+\frac{151+24\pi^2}{288}\frac{\kappa^2}{s^2}\right], \tag{A46}$$

$$d_{0001}=-4+\rho_2, \tag{A47}$$

$$d_{2000}=(2\rho_1+\rho_2)\frac{16}{9\pi}\frac{\kappa^2}{s}, \tag{A48}$$

$$d_{0200}=(\rho_1-\rho_2)\frac{\pi}{4}\frac{\kappa^2}{s}, \tag{A49}$$

$$d_{1100}=\rho_1\frac{45\pi^2-128}{90\pi}\frac{\kappa^2}{s}+\rho_2\left[\frac{32}{15\pi}\frac{1-\eta}{1+\eta}s-\frac{9\pi^2-64}{18\pi}\frac{\kappa^2}{s}\right], \tag{A50}$$

$$d_{0020}=\rho_2\frac{64}{3\pi}\frac{\kappa^2}{s}, \tag{A51}$$

$$d_{0011}=\rho_2\frac{128}{15\pi}\left[\frac{s}{1+\eta}+\frac{\kappa^2}{s}\right], \tag{A52}$$

$$d_{2001}=\frac{7}{4}-\rho_1\left[\frac{1}{2(1+\eta)}-\frac{10}{9}\frac{\kappa^2}{s^2}\right]+\rho_2\left[\frac{\eta}{2(1+\eta)}+\frac{\kappa^2}{18s^2}\right] \tag{A53}$$

$$d_{0201}=\frac{5}{3}-\rho_1\left[\frac{3}{4(1+\eta)}+\frac{45+16\pi^2}{192}\frac{\kappa^2}{s^2}\right]+\rho_2\left[\frac{3\eta}{4(1+\eta)}+\frac{45+16\pi^2}{192}\frac{\kappa^2}{s^2}\right], \tag{A54}$$

$$d_{0021}=\frac{5}{6}+\rho_2\left[\frac{2\eta-1}{1+\eta}+\frac{17}{12}\frac{\kappa^2}{s^2}\right], \tag{A55}$$

$$d_{0003}=\frac{2}{3}+\rho_2\left[\frac{2\eta-1}{2(1+\eta)}+\frac{5}{8}\frac{\kappa^2}{s^2}\right], \tag{A56}$$

$$d_{2010}=-\left(\frac{43}{18}\rho_1+\frac{13}{9}\rho_2\right)\frac{\kappa^2}{s^2}, \tag{A57}$$

$$d_{0210}=-(\rho_1-\rho_2)\frac{16}{9}\frac{\kappa^2}{s^2}, \tag{A58}$$

$$d_{0030}=-\rho_2\frac{29}{3}\frac{\kappa^2}{s^2}, \tag{A59}$$

$$d_{0012} = -\rho_2 \frac{2}{3} \frac{\kappa^2}{s^2}, \tag{A60}$$

$$d_{1101} = -\left(\rho_1 + \frac{1}{3}\rho_2\right)\frac{\kappa^2}{s^2}, \tag{A61}$$

$$d_{1110} = -\frac{5}{12} - \rho_1\left[\frac{1}{1+\eta} + \frac{487+24\pi^2}{288}\frac{\kappa^2}{s^2}\right] + \rho_2\left[\frac{\eta}{1+\eta} + \frac{67+24\pi^2}{288}\frac{\kappa^2}{s^2}\right]. \tag{A62}$$

[1] N.V. Tabiryan, A.V. Sukhov, and B.Y. Zel'dovich, Mol. Cryst. Liq. Cryst. **136**, 1 (1986).

[2] I.C. Khoo and S.T. Wu, *Optics and Nonlinear Optics of Liquid Crystals* (World Scientific, Singapore, 1993).

[3] F. Simoni, *Nonlinear Optical Properties of Liquid Crystals and PDLC* (World Scientific, Singapore, 1997).

[4] S. Arakelyan, Sov. Phys. Usp. **30**, 1041 (1987).

[5] E. Santamato, B. Daino, M. Romagnoli, M. Settembre, and Y.R. Shen, Phys. Rev. Lett. **57**, 2423 (1986).

[6] E. Santamato, G. Abbate, P. Maddalena, L. Marrucci, and Y.R. Shen, Phys. Rev. Lett. **64**, 1377 (1990).

[7] A. Vella, B. Piccirillo, and E. Santamato, Phys. Rev. E **65**, 031706 (2002).

[8] E. Brasselet, B. Doyon, T.V. Galstian, and L.J. Dubé, Phys. Lett. A **299**, 212 (2002).

[9] E. Brasselet, B. Doyon, T.V. Galstian, and L.J. Dubé, Phys. Rev. E **67**, 031706 (2003).

[10] E. Brasselet, B. Doyon, T.V. Galstian, and L.J. Dubé, Phys. Rev. E **69**, 021701 (2004).

[11] E. Santamato, P. Maddalena, L. Marrucci, and B. Piccirillo, Liq. Cryst. **25**, 357 (1998).

[12] G. Demeter and L. Kramer, Phys. Rev. Lett. **83**, 4744 (1999).

[13] V. Carbone, G. Cipparrone, and G. Russo, Phys. Rev. E **63**, 051701 (2001).

[14] T.V. Galstyan and V. Drnoyan, Phys. Rev. Lett. **78**, 2760 (1997).

[15] E. Brasselet and T.V. Galstian, Opt. Commun. **200**, 241 (2001).

[16] E. Brasselet and T.V. Galstian, J. Opt. Soc. Am. B **18**, 982 (2001).

[17] G. Russo, G. Cipparrone, and V. Carbone, Europhys. Lett. **63**, 180 (2003).

[18] B.Y. Zel'dovich and N. Tabiryan, Zh. Eksp. Teor. Fiz. **82**, 1126 (1982) [Sov. Phys. JETP **55**, 656 (1982)].

[19] G. Demeter, Phys. Rev. E **61**, 6678 (2000).

[20] E. Ott, C. Grebogi, and J.A. Yorke, Phys. Rev. Lett. **64**, 1196 (1990).

[21] K. Pyragas, Phys. Lett. A **170**, 421 (1992).